Inferred Cosmic-Ray Spectrum from Fermi Large Area Telescope γ-Ray Observations of Earth's Limb

M. Ackermann,[1] M. Ajello,[2] A. Albert,[3] A. Allafort,[3] L. Baldini,[4] G. Barbiellini,[5,6] D. Bastieri,[7,8] K. Bechtol,[3] R. Bellazzini,[4] R. D. Blandford,[3] E. D. Bloom,[3] E. Bonamente,[9,10] E. Bottacini,[3] A. Bouvier,[11] T. J. Brandt,[12] M. Brigida,[13,14] P. Bruel,[15] R. Buehler,[1] S. Buson,[7,8] G. A. Caliandro,[3,16] R. A. Cameron,[3] P. A. Caraveo,[17] C. Cecchi,[9,10] E. Charles,[3] R. C. G. Chaves,[18] A. Chekhtman,[19,*] J. Chiang,[3] G. Chiaro,[8] S. Ciprini,[20,21] R. Claus,[3] J. Cohen-Tanugi,[22] J. Conrad,[23,24,25] S. Cutini,[20,21] M. Dalton,[26] F. D'Ammando,[27] A. de Angelis,[28] F. de Palma,[13,14] C. D. Dermer,[29] S. W. Digel,[3] L. Di Venere,[13] E. do Couto e Silva,[3] P. S. Drell,[3] A. Drlica-Wagner,[30] C. Favuzzi,[13,14] S. J. Fegan,[15] E. C. Ferrara,[12] W. B. Focke,[3] A. Franckowiak,[3] Y. Fukazawa,[31] S. Funk,[3,†] P. Fusco,[13,14] F. Gargano,[14] D. Gasparrini,[20,21] S. Germani,[9,10] N. Giglietto,[13,14] F. Giordano,[13,14] M. Giroletti,[27] T. Glanzman,[3] G. Godfrey,[3] G. A. Gomez-Vargas,[32,33,34] I. A. Grenier,[18] J. E. Grove,[29] S. Guiriec,[12] M. Gustafsson,[35] D. Hadasch,[36] Y. Hanabata,[37] A. K. Harding,[12] M. Hayashida,[37] K. Hayashi,[38] J. W. Hewitt,[12] D. Horan,[15] X. Hou,[26] R. E. Hughes,[39] Y. Inoue,[3] M. S. Jackson,[40,24] T. Jogler,[3] G. Jóhannesson,[41] A. S. Johnson,[3] T. Kamae,[3] T. Kawano,[31] J. Knödlseder,[42,43] M. Kuss,[4] J. Lande,[3] S. Larsson,[23,24,44] L. Latronico,[45] F. Longo,[5,6] F. Loparco,[13,14] M. N. Lovellette,[29] P. Lubrano,[9,10] M. Mayer,[1] M. N. Mazziotta,[14] J. E. McEnery,[12,46] J. Mehault,[26] P. F. Michelson,[3] W. Mitthumsiri,[3,47,‡] T. Mizuno,[48] A. A. Moiseev,[49,46] C. Monte,[13,14] M. E. Monzani,[3] A. Morselli,[32] I. V. Moskalenko,[3,§] S. Murgia,[50] R. Nemmen,[12,49,51] E. Nuss,[22] T. Ohsugi,[48] A. Okumura,[3,52] M. Orienti,[27] E. Orlando,[3] J. F. Ormes,[53] D. Paneque,[54,3] J. H. Panetta,[3] J. S. Perkins,[12] M. Pesce-Rollins,[4] F. Piron,[22] G. Pivato,[8] T. A. Porter,[3] S. Rainò,[13,14] R. Rando,[7,8] M. Razzano,[4] S. Razzaque,[55] A. Reimer,[36,3] O. Reimer,[36,3] S. Ritz,[11] M. Roth,[56] M. Schaal,[57,*] A. Schulz,[1] C. Sgrò,[4] E. J. Siskind,[58] G. Spandre,[4] P. Spinelli,[13,14] A. W. Strong,[59] H. Takahashi,[31] Y. Takeuchi,[60] J. G. Thayer,[3] J. B. Thayer,[3] D. J. Thompson,[12] L. Tibaldo,[3] M. Tinivella,[4] D. F. Torres,[61,62] G. Tosti,[9,10] E. Troja,[12,46] V. Tronconi,[8] T. L. Usher,[3] J. Vandenbroucke,[3] V. Vasileiou,[22] G. Vianello,[3] V. Vitale,[32,63] M. Werner,[36] B. L. Winer,[39] K. S. Wood,[29] M. Wood,[3] and Z. Yang[23,24]

(Fermi LAT Collaboration)

[1]*Deutsches Elektronen Synchrotron DESY, D-15738 Zeuthen, Germany*
[2]*Space Sciences Laboratory, 7 Gauss Way, University of California, Berkeley, California 94720-7450, USA*
[3]*W. W. Hansen Experimental Physics Laboratory, Kavli Institute for Particle Astrophysics and Cosmology, Department of Physics and SLAC National Accelerator Laboratory, Stanford University, Stanford, California 94305, USA*
[4]*Istituto Nazionale di Fisica Nucleare, Sezione di Pisa, I-56127 Pisa, Italy*
[5]*Istituto Nazionale di Fisica Nucleare, Sezione di Trieste, I-34127 Trieste, Italy*
[6]*Dipartimento di Fisica, Università di Trieste, I-34127 Trieste, Italy*
[7]*Istituto Nazionale di Fisica Nucleare, Sezione di Padova, I-35131 Padova, Italy*
[8]*Dipartimento di Fisica e Astronomia "G. Galilei", Università di Padova, I-35131 Padova, Italy*
[9]*Istituto Nazionale di Fisica Nucleare, Sezione di Perugia, I-06123 Perugia, Italy*
[10]*Dipartimento di Fisica, Università degli Studi di Perugia, I-06123 Perugia, Italy*
[11]*Santa Cruz Institute for Particle Physics, Department of Physics and Department of Astronomy and Astrophysics, University of California at Santa Cruz, Santa Cruz, California 95064, USA*
[12]*NASA Goddard Space Flight Center, Greenbelt, Maryland 20771, USA*
[13]*Dipartimento di Fisica "M. Merlin" dell'Università e del Politecnico di Bari, I-70126 Bari, Italy*
[14]*Istituto Nazionale di Fisica Nucleare, Sezione di Bari, 70126 Bari, Italy*
[15]*Laboratoire Leprince-Ringuet, École polytechnique, CNRS/IN2P3, Palaiseau, France*
[16]*Consorzio Interuniversitario per la Fisica Spaziale (CIFS), I-10133 Torino, Italy*
[17]*INAF-Istituto di Astrofisica Spaziale e Fisica Cosmica, I-20133 Milano, Italy*
[18]*Laboratoire AIM, CEA-IRFU/CNRS/Université Paris Diderot, Service d'Astrophysique, CEA Saclay, 91191 Gif sur Yvette, France*
[19]*Center for Earth Observing and Space Research, College of Science, George Mason University, Fairfax, Virginia 22030, USA*
[20]*Agenzia Spaziale Italiana (ASI) Science Data Center, I-00044 Frascati (Roma), Italy*
[21]*Istituto Nazionale di Astrofisica - Osservatorio Astronomico di Roma, I-00040 Monte Porzio Catone (Roma), Italy*
[22]*Laboratoire Univers et Particules de Montpellier, Université Montpellier 2, CNRS/IN2P3 Montpellier, France*
[23]*Department of Physics, Stockholm University, AlbaNova, SE-106 91 Stockholm, Sweden*
[24]*The Oskar Klein Centre for Cosmoparticle Physics, AlbaNova, SE-106 91 Stockholm, Sweden*
[25]*The Royal Swedish Academy of Sciences, Box 50005, SE-104 05 Stockholm, Sweden*

[26]Centre d'Études Nucléaires de Bordeaux Gradignan, IN2P3/CNRS, Université Bordeaux 1, BP120, F-33175 Gradignan Cedex, France
[27]INAF Istituto di Radioastronomia, 40129 Bologna, Italy
[28]Dipartimento di Fisica, Università di Udine and Istituto Nazionale di Fisica Nucleare, Sezione di Trieste, Gruppo Collegato di Udine, I-33100 Udine, Italy
[29]Space Science Division, Naval Research Laboratory, Washington, D.C. 20375-5352, USA
[30]Fermilab, Batavia, Illinois 60510, USA
[31]Department of Physical Sciences, Hiroshima University, Higashi-Hiroshima, Hiroshima 739-8526, Japan
[32]Istituto Nazionale di Fisica Nucleare, Sezione di Roma "Tor Vergata", I-00133 Roma, Italy
[33]Departamento de Física Teórica, Universidad Autónoma de Madrid, Cantoblanco, E-28049 Madrid, Spain
[34]Instituto de Física Teórica IFT-UAM/CSIC, Universidad Autónoma de Madrid, Cantoblanco, E-28049 Madrid, Spain
[35]Service de Physique Theorique, Universite Libre de Bruxelles (ULB), Bld du Triomphe, CP225, 1050 Brussels, Belgium
[36]Institut für Astro- und Teilchenphysik and Institut für Theoretische Physik, Leopold-Franzens-Universität Innsbruck, A-6020 Innsbruck, Austria
[37]Institute for Cosmic-Ray Research, University of Tokyo, 5-1-5 Kashiwanoha, Kashiwa, Chiba 277-8582, Japan
[38]Institute of Space and Astronautical Science, JAXA, 3-1-1 Yoshinodai, Chuo-ku, Sagamihara, Kanagawa 252-5210, Japan
[39]Department of Physics, Center for Cosmology and Astro-Particle Physics, The Ohio State University, Columbus, Ohio 43210, USA
[40]Department of Physics, KTH Royal Institute of Technology, AlbaNova, SE-106 91 Stockholm, Sweden
[41]Science Institute, University of Iceland, IS-107 Reykjavik, Iceland
[42]CNRS, IRAP, F-31028 Toulouse cedex 4, France
[43]GAHEC, Université de Toulouse, UPS-OMP, IRAP, 31028 Toulouse, France
[44]Department of Astronomy, Stockholm University, SE-106 91 Stockholm, Sweden
[45]Istituto Nazionale di Fisica Nucleare, Sezione di Torino, I-10125 Torino, Italy
[46]Department of Physics and Department of Astronomy, University of Maryland, College Park, Maryland 20742, USA
[47]Department of Physics, Faculty of Science, Mahidol University, Bangkok 10400, Thailand
[48]Hiroshima Astrophysical Science Center, Hiroshima University, Higashi-Hiroshima, Hiroshima 739-8526, Japan
[49]Center for Research and Exploration in Space Science and Technology (CRESST) and NASA Goddard Space Flight Center, Greenbelt, Maryland 20771, USA
[50]Center for Cosmology, Physics and Astronomy Department, University of California, Irvine, California 92697-2575, USA
[51]Department of Physics and Center for Space Sciences and Technology, University of Maryland Baltimore County, Baltimore, Maryland 21250, USA
[52]Solar-Terrestrial Environment Laboratory, Nagoya University, Nagoya 464-8601, Japan
[53]Department of Physics and Astronomy, University of Denver, Denver, Colorado 80208, USA
[54]Max-Planck-Institut für Physik, D-80805 München, Germany
[55]Department of Physics, University of Johannesburg, PO Box 524, Auckland Park 2006, South Africa
[56]Department of Physics, University of Washington, Seattle, Washington 98195-1560, USA
[57]National Research Council Research Associate, National Academy of Sciences, Washington, D.C. 20001, USA
[58]NYCB Real-Time Computing Inc., Lattingtown, New York 11560-1025, USA
[59]Max-Planck Institut für extraterrestrische Physik, 85748 Garching, Germany
[60]Research Institute for Science and Engineering, Waseda University, 3-4-1, Okubo, Shinjuku, Tokyo 169-8555, Japan
[61]Institut de Ciències de l'Espai (IEEE-CSIC), Campus UAB, 08193 Barcelona, Spain
[62]Institució Catalana de Recerca i Estudis Avançats (ICREA), Barcelona, Spain
[63]Dipartimento di Fisica, Università di Roma "Tor Vergata", I-00133 Roma, Italy

(Received 13 December 2013; published 17 April 2014)

Recent accurate measurements of cosmic-ray (CR) species by ATIC-2, CREAM, and PAMELA reveal an unexpected hardening in the proton and He spectra above a few hundred GeV, a gradual softening of the spectra just below a few hundred GeV, and a harder spectrum of He compared to that of protons. These newly discovered features may offer a clue to the origin of high-energy CRs. We use the Fermi Large Area Telescope observations of the γ-ray emission from Earth's limb for an indirect measurement of the local spectrum of CR protons in the energy range ~90 GeV–6 TeV (derived from a photon energy range 15 GeV–1 TeV). Our analysis shows that single power law and broken power law spectra fit the data equally well and yield a proton spectrum with index 2.68 ± 0.04 and 2.61 ± 0.08 above ~200 GeV, respectively.

DOI: 10.1103/PhysRevLett.112.151103 PACS numbers: 96.50.sb, 95.85.Pw, 95.85.Ry, 98.70.Sa

Introduction.—The spectrum of cosmic rays (CRs) has offered few clues to its origin so far. The generally accepted features are at very-high and ultrahigh energies (see, e.g., Fig. 1 in [1]): the so-called "knee" at a few thousand TeV [2,3], the second "knee" at $\sim 10^6$ TeV, the "ankle" at higher energies [4], and a spectral steepening above 10^8 TeV [5,6]. It is believed that CRs below the second knee are Galactic, while extragalactic CRs dominate at higher energies [7,8].

The data recently collected by three experiments, ATIC-2 [9,10], CREAM [11,12], and PAMELA [13], indicate a new feature at relatively low energy: a break (or hardening) of CR proton and He spectra at ~240 GV in rigidity. PAMELA claims to detect the break at 95% confidence level for both species. Below the break, PAMELA data agree very well with the earlier data from AMS-01 [14] and BESS [15]. Above the break, ATIC-2 results agree well with those of CREAM, smoothly connecting to highest energy points from PAMELA. The change in the spectral indices for both protons and He is ~0.2.

However, the break itself is observed only by PAMELA near its high-energy limit. Much evidence of this newly discovered break or flattening comes from a combination of data by several different experiments, which may be subject to cross-calibration errors. A verification of this new feature requires an independent confirmation, preferably with a single instrument. Meanwhile, recent preliminary AMS-02 results [16] do not show any feature in the proton and He spectra up to ~2 TeV and also seem to contradict ATIC-2 and CREAM results. In this Letter, we demonstrate that such a measurement can also be done indirectly through observation of the CR-induced γ-ray emission from Earth's atmosphere.

Atmospheric γ-ray emission is mainly the result of hadronic CR cascades: CRs entering the atmosphere near grazing incidence produce showers that develop in the forward direction, resulting in a very bright γ-ray signal from Earth's limb as seen from orbit. The γ-ray spectrum from CR interactions at the very top of the atmosphere depends only on the inclusive γ-ray production cross section and the spectrum of CR particles. If the cross section is known, the shape of the local CR spectrum can be recovered from the γ-ray spectrum. However, this method can only measure the total spectrum of CRs. To deduce the spectrum of protons, the most abundant component of CRs, one has to assume a spectrum of He, the second most abundant component. The contribution of the latter to the total γ-ray emission is ~10–20%, depending on the energy. Therefore, accurate modeling of the contribution from He interactions is not very critical, and heavier nuclei can be neglected.

Observations of Galactic diffuse γ-ray emission (GDE) have provided valuable information about CR spectra in distant locations [17–21] and in the local interstellar medium [22,23]. Similarly, observations of Earth's limb γ-ray emission can be used to deduce the CR spectrum near Earth. In contrast with the GDE, the contribution from the inverse Compton scattering of CR electrons to Earth's limb emission is negligible. Furthermore, viewed from low-Earth orbit, the limb is orders of magnitude brighter than the GDE. Using Earth's emission is, therefore, a simpler way to derive the spectrum of CR nucleons than using the GDE.

The γ-ray emission from Earth's limb was first observed by the SAS-2 [24] and EGRET [25] instruments, but these observations were limited in statistics and angular resolution. Fermi LAT made the first measurement of Earth's limb γ-ray emission above 10 GeV [26] and was able to resolve the limb profile to discriminate between the thin and thick target regimes, demonstrating its capability for indirect measurements of the CR spectrum. In this Letter, we report on the analysis of 5 years of Earth's limb observations with the Fermi large area telescope (LAT).

Data and Analysis Method.—Fermi was launched in June 2008 and spent the first few weeks calibrating the instruments during the launch and early operations (LEO) period, during which the LAT was tracking a few well-known bright sources, allowing Earth's limb to frequently enter the field of view. In September 2008, three hours of limb-stare observations were performed. This is the data set used in [26] and part of the data set in the analysis presented here. The additional part of the data set is described as follows.

The spacecraft operates mainly in survey mode, keeping Earth's limb far from its boresight as it is a background for other analyses. However, for a small fraction of the operating time, the LAT performs pointed observations by following a celestial target while it is not occulted by Earth, including while it is near the limb. We select this pointed data set by accepting events when the magnitude of the rocking angle [27] is $> 52°$, 2° greater than that for the normal survey mode, up to August 8, 2013. This rocking angle selection rejects the survey mode data, for which Earth's limb photons have large ($> 62°$) incidence angle.

We avoid the geomagnetic and solar modulation of local CRs near Earth by considering only γ rays above 15 GeV because they must be produced by CR protons with energies of at least (but mostly much greater than) 15 GeV. The resulting number of Earth's limb photons above 15 GeV ($N_{>15\ \mathrm{GeV}}$) and the average incidence angles measured from the LAT's boresight ($\langle\Theta_{\mathrm{LAT}}\rangle$) for these data sets are in Table I.

The data are analyzed here in the local nadir coordinates, in which Θ_{Nadir} is the angle measured from the nadir direction at the location of the LAT. At the LAT's altitude of ~565 km, the physical limb of Earth is at $\Theta_{\mathrm{Nadir}} \approx 66.7°$. However, the peak of the γ-ray emission above 15 GeV is at $\Theta_{\mathrm{Nadir}} \approx 68.1°$, due to the height of the atmosphere and the effects of γ-ray absorption as discussed in detail in [26]. At $\Theta_{\mathrm{Nadir}} = 68.4°$, the integrated column density for grazing-incidence particles is ~3 $g\,\mathrm{cm}^{-2}$ (see Fig. 5 in [26]). From this angle outwards, the atmosphere is in the thin-target regime with photons produced from a single interaction, the

TABLE I. Observation types and durations for this analysis.

Observation type	Start date	End date	Live time (days)	$\langle\Theta_{\rm LAT}\rangle$	$N_{>15\ {\rm GeV}}$
LEO	Jul 15, 2008	Jul 30, 2008	9	44°	967
Limb stare	Sep 29, 2008	Sep 29, 2008	0.125	31°	18
Pointed (multiple)	Aug 21, 2008	Aug 8, 2013	90	45°	6762

absorption effects are negligible, and the resulting γ-ray spectrum is determined by the local spectrum of CRs. Thus, $\Theta_{\rm Nadir} = 68.4°$ is the inner edge for the studies presented here. The outer edge of Earth's limb is chosen as $\Theta_{\rm Nadir} = 70.0°$ because the emission from celestial sources starts to dominate for larger $\Theta_{\rm Nadir}$ angles.

We use the P7REP reprocessed data (see [28] and Fermi Science Support Center page [29] for details) with the P7REP_SOURCE event selection and the associated P7REP_SOURCE_V15 instrument response functions. We apply two additional cuts: $\Theta_{\rm LAT} < 70°$ (reduced incidence angle) to avoid the edge of the field of view, which is prone to systematic uncertainties, and $68.4° < \Theta_{\rm Nadir} < 70°$ (thin-target regime) to select photons from Earth's limb.

The background is estimated from a ring surrounding Earth's limb ($80° < \Theta_{\rm Nadir} < 90°$). The ring immediately surrounding the limb was not used in order to avoid spill-over photons from the limb due to the LAT's point-spread function (PSF). The background level shown in Fig. 1 is small, ranging from ~3% at 15 GeV to ~5%at 500 GeV of the bright limb emission.

For the P7REP data used here, dedicated simulations and flight data comparisons have been performed to validate the LAT responses up to 1 TeV by the LAT Collaboration. Based on these studies, we adopt an effective area ($A_{\rm eff}$) uncertainty of 5% at 10 GeV, increasing linearly with the logarithm of energy to 15% at 1 TeV [30].

We simulate many realizations of the energy dependence of the $A_{\rm eff}$ which obey the above estimated uncertainty to observe the effect of instrumental systematic error. Specifically, to obtain one realization, we generate three random numbers at 10, 100, and 1000 GeV from Gaussian distributions for which the mean is 0 and σ is the value of the uncertainty estimation at the three energy points. Cubic spline interpolation between these points describes the deviation of $A_{\rm eff}$ from the central value, which would then distort Earth's measured limb spectrum in a way consistent with the systematic uncertainties, allowing us to evaluate the propagated uncertainties of the final results. This algorithm to simulate $A_{\rm eff}$ uncertainties assumes uncorrelated errors for two energy bins that are sufficiently far apart (larger than half a decade in energy), but the interpolation results in highly correlated errors between nearby energy bins (see Section 5.6.2 in [31]).

We also correct for the angular resolution effects on the limb spectrum itself. The dominant effect is contamination by limb photons from $\Theta_{\rm Nadir} < 68.4°$, where the emission is brighter. The other is the leakage of photons from the limb to each side of the defined boundary. Above 15 GeV, where the LAT's PSF is narrow (68% containment at ~0.2°) and not strongly energy dependent (see Fig. 57 in [31]), these corrections, combined, decrease the measured intensities by ~35%, depending on energy. The effect on the spectral index is relatively small compared to that from $A_{\rm eff}$.

We determined that $+2\%/-5\%$ uncertainty of the absolute energy scale (described in Section 7.3.4 in [31]) translates into < 10% effects on the absolute normalization of the spectrum, which does not alter the results presented here.

To infer the CR proton spectrum from the γ-ray measurement, we use two $pp \to \gamma$ interaction models, one by Kamae *et al.* [32] (Kamae model) and the other by Kachelrieß and Ostapchenko [35] (KO model). For each model, we calculate the γ-ray spectrum by integrating a model of the proton spectrum from ~0.5 GeV to ~500 TeV in kinetic energy.

In our study, we assume that the atmosphere consists of 100% Nitrogen. This does not affect our results because studies of proton-nucleus interactions at high energies (e.g., [33,34]) show that the pA cross section can be scaled from the pp cross section by applying an energy-independent scaling factor $\propto A^{0.7}$, where A is the atomic number of the nucleus. The precise scaling factor for the atmospheric composition is not important for this analysis because it changes only the normalization of the fitted proton spectrum.

Observations of the γ-ray emission from Earth's limb cannot discriminate between contributions of CR protons and heavier nuclei. Thus, we must rely on the direct measurements of the CR composition. The He fraction in CRs is about 6%–10% by number, depending on energy, in our energy range of interest, so its contribution has to be taken into account, while the contribution of the heavier nuclei can be safely neglected. There are a number of empirical parametrizations for nucleus-nucleus meson multiplicity (e.g., Appendix A in [33] and Eq. (3b) in [34]). These formulas give similar values for the ratio of αN to pN cross sections, $\sigma_{\alpha N}/\sigma_{pN} \sim 1.6$. We use this number to scale the pp-interaction models and to calculate the relative contribution of He nuclei to the limb γ-ray emission. Since the contribution of γ rays produced by He is ~10%–20% depending on energy, and most of the emission is produced by protons, the αN scaling uncertainty has little influence on the final fit results.

To determine the He spectrum, we fit the combined PAMELA ([13]), CREAM ([12]), and ATIC-2 ([10])

He data above 50 GeV/n (102 GV) with spectral forms described below Eq. (1). According to PAMELA measurements [13], the He/p ratio at ~90 GeV is 6.2%. We use this value together with the cross section scaling to fix the contribution of He to photon production at 15 GeV to 9.5%. We then forward fold by varying the parameters of the input proton spectrum so that the resulting γ-ray spectrum calculated from the pp-interaction models provides the best fit to Earth's limb measurement. In the fitting procedure, the normal Poisson likelihood function is maximized

$$L = \prod_{i=1}^{N} P_{\text{Poisson}}(n_i^{\text{obs}}, n_i^{\text{mod}}), \quad (1)$$

where N is the number of energy bins. P_{Poisson} is the Poisson probability of observing n_i^{obs} counts given that the model predicts n_i^{mod} counts (γ-ray model flux × exposure) for the ith energy bin. We use two models for the local CR proton and He spectra in the fitting procedure: (i) Single power law in rigidity (SPL). This model assumes a single power law for CR protons and He. For He, the index 2.73 ± 0.01 is our best-fit value of the combined PAMELA, CREAM, and ATIC-2 data. For protons, we fit both the normalization and index to our measurement of the γ-ray spectrum from Earth's limb. (ii) Broken power law in rigidity (BPL). This model assumes a broken power law for both proton and He spectra. As before, the He spectrum is fixed to the best fit of the combined direct measurements, for which the spectral index changes from 2.82 ± 0.07 to 2.55 ± 0.02 at 247 ± 44 GV. We then fit the indices, break energy (E_{break}), and normalization for the proton spectrum.

We evaluate the statistical uncertainties of the fit results by fitting a large number of simulated realizations of photon counts generated with a Poisson distribution for which the expected value is the measured count in each energy bin. Likewise, simultaneous simulations of photon counts and ranges of A_{eff}, as previously described, give the total (combined systematic and statistical) errors. We also add in quadrature the 5% absolute energy scale uncertainty to the errors of the fitted energy parameter.

Results.—The measured γ-ray thin-target limb spectrum, the background-sky flux (which has already been subtracted from the limb spectrum), and the best-fit γ-ray models are shown in Fig. 1. The γ-ray emission from the local neutral atomic hydrogen (HI) [36] is scaled to approximately match that from Earth's limb and is shown for comparison. As expected, the two agree well above ~10 GeV, since they are produced from hadronic interactions by the same local population of CRs in the thin-target regime. Below ~10 GeV, the spectra differ due to the geomagnetic and solar modulations of CRs in the vicinity of Earth, reducing the number of CRs interacting with Earth's atmosphere. For this reason we limited our study to limb γ rays above 15 GeV. The approximate proton-to-γ-ray energy conversion factor for the power-law spectrum of

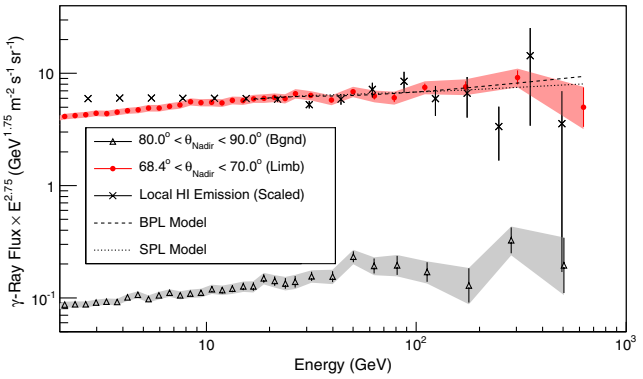

FIG. 1 (color online). The γ-ray energy spectra multiplied by $E^{2.75}$. The background-sky spectrum (triangles) has been subtracted from the limb spectrum (circles). The scaled local HI emission (crosses) is shown for comparison. Best-fit γ-ray results from two CR models based on the KO model [35] are also plotted as dotted and dashed lines. Statistical and total (quadrature sum of statistical and systematic) errors are shown as bars and bands, respectively.

protons is 0.17 [37]. The energy range of the inferred proton spectrum is, thus, ~90 GeV–6 TeV.

Using the KO and Kamae models, we obtain the results shown in Table II. The log likelihood for the best-fit BPL is ~0.9 better than that for the best-fit SPL. To account for A_{eff} systematic uncertainties, we apply Monte Carlo simulations to translate this likelihood ratio into a significance. By assuming that the best-fit SPL is the true underlying flux model, we produce ~2000 simulations of A_{eff} from the estimated errors as previously discussed, for each of which we generate ~1000 simulations of SPL realizations. We then fit the distribution of the log likelihood differences between SPL and BPL for these ~$2M$ total simulations with a Gaussian function and evaluate how likely it is that the best-fit BPL we obtain from the actual measurement would give a log likelihood difference of 0.9 or above as compared to the SPL. We find that it corresponds to a significance of 1.0σ.

We performed several cross checks to test the stability and consistency of the results. We studied the effects of using the event selection with more stringent rejection of residual CRs (P7REP_CLEAN), tighter incidence angle (Θ_{LAT}) cuts, and reasonable variations of the fitted energy

TABLE II. Fit results from Kamae [32] and KO [35] models, shown as value ± total error (statistical error).

	Kamae	KO
SPL index	2.67 ± 0.05 (0.03)	2.68 ± 0.04 (0.03)
BPL index 1	2.81 ± 0.10 (0.03)	2.81 ± 0.11 (0.04)
BPL index 2	2.60 ± 0.08 (0.05)	2.61 ± 0.08 (0.06)
BPL E_{break}	276 ± 64 (55) GeV	302 ± 96 (62) GeV
BPL vs SPL	1.0σ	1.0σ

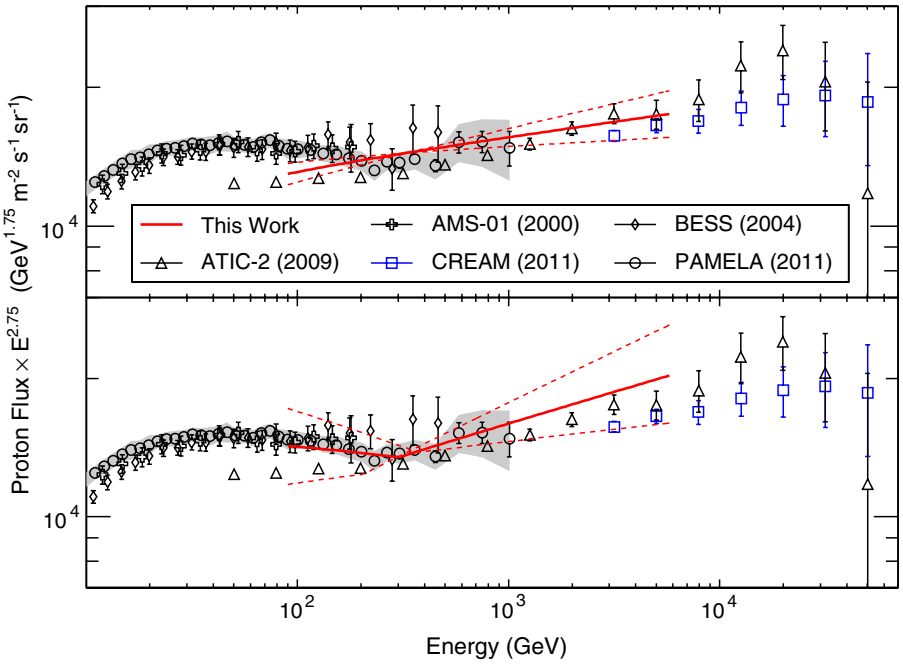

FIG. 2 (color online). Best-fit single power law or SPL (top), and best-fit broken power law or BPL (bottom) spectrum for the local CR proton spectrum (solid red lines) as derived from Earth's limb γ-ray data using the KO model [35] for pp interactions. The total (combined statistical and systematic, neglecting errors in absolute normalization) uncertainties are the dashed red lines. Other direct measurements ([10,12–15]) are shown for comparison. The gray band is PAMELA's total uncertainty.

ranges (up to 20 GeV lower bound and down to 120 GeV upper bound in γ-ray energy). All of these cases yield consistent results.

Figure 2 shows the resulting best-fit SPL and BPL derived from the KO model in comparison with direct measurements, assuming an effective atmospheric column density of $\sim 1.0\ g\,\mathrm{cm}^{-2}$, as described below.

In order to determine the absolute normalization of the inferred proton spectrum, we use the NRLMSISE-00 atmospheric model [38] to calculate the average line-of-sight column density, weighted by γ-ray intensity, in the range studied here ($\Theta_{\mathrm{Nadir}} = 68.40°$–$70.00°$) to be $1.2\ g\,\mathrm{cm}^{-2}$. Because of the exponential change of the atmospheric density with Θ_{Nadir}, the evaluated density is extremely sensitive to the lower bound of the Θ_{Nadir} range. Thus, we empirically adjust the absolute normalization of our inferred proton spectrum to approximately match that of direct measurements as shown in Fig. 2 by changing the atmospheric column density from 1.2 to $1.0\ g\,\mathrm{cm}^{-2}$. This is equivalent to increasing the lower bound of Θ_{Nadir} from 68.40° to 68.42° when we calculate the atmospheric column density. The small change in the effective lower bound of Θ_{Nadir} by ∼0.02° has many potential justifications, such as the LAT altitude variations which smear the precise calculation of the target density, the atmospheric model uncertainties, and other absolute normalization uncertainties as previously discussed. Since our primary interest is in the spectral indices, the difference in normalization is of no importance.

Discussion and conclusion.—Our LAT analysis, which employs a different technique from direct measurements, shows that the CR proton spectrum between ∼90 GeV and 6 TeV can be described equally well ($\sim 1\sigma$) with the SPL and BPL models. The best-fit spectral indices (2.68 ± 0.04 for SPL and 2.61 ± 0.08 above ∼200 GeV for BPL) are consistent with each other.

We note that our best-fit SPL index is $\sim 3\sigma$ from the value (2.801 ± 0.007) reported by PAMELA for a lower energy range (29–79 GeV). However, our best-fit SPL index for ∼90 GeV–6 TeV is in good agreement with the fitted index for ∼230 GeV–1 TeV reported by PAMELA [13] and with the measurements at higher energies by ATIC-2 [10] and CREAM [12]. While Fermi LAT results cannot confirm or disprove the existence of the spectral break itself yet, they do indicate a flatter proton spectrum at high energies, consistent with direct measurements by ATIC-2 and CREAM.

This result is the first indirect measurement of the proton spectrum in the energy range ∼90 GeV–6 TeV using observations of the γ-ray emission of Earth's limb. Continuing observations with Fermi LAT will allow us to improve the precision of the measurement of the CR spectrum and extend the energy range.

The Fermi LAT Collaboration acknowledges support from a number of agencies and institutes for both the

development and the operation of the LAT as well as scientific data analysis. These include NASA and DOE in the United States, CEA/Irfu and IN2P3/CNRS in France, ASI and INFN in Italy, MEXT, KEK, and JAXA in Japan, and the K. A. Wallenberg Foundation, the Swedish Research Council and the National Space Board in Sweden. Additional support from INAF in Italy and CNES in France for science analysis during the operations phase is gratefully acknowledged. I.V.M. acknowledges support from NASA Grants No. NNX11AQ06 G and No. NNX13AC47 G. Royal Swedish Academy of Sciences Research Fellow J. Conrad, funded by a grant from the K. A. Wallenberg Foundation, NASA Postdoctoral Program Fellow S. Guiriec, USA. M. Razzano Funded by Contract No. FIRB-2012-RBFR12PM1 F from the Italian Ministry of Education, University and Research (MIUR).

[*]Present address: Naval Research Laboratory, Washington, D.C. 20375, USA.
[†]funk@slac.stanford.edu
[‡]warit.mit@mahidol.ac.th
[§]imos@stanford.edu

[1] S. P. Swordy, Space Sci. Rev. **99**, 85 (2001).
[2] G. V. Kulikov and G. B. Khristiansen, Sov. Phys. JETP **35**, 635 (1958).
[3] A. Haungs, H. Rebel, and M. Roth, Rep. Prog. Phys. **66**, 1145 (2003).
[4] R. U. Abbasi *et al.*, Phys. Lett. B **619**, 271 (2005).
[5] R. U. Abbasi *et al.*, Astropart. Phys. **32**, 53 (2009).
[6] J. Abraham *et al.*, Phys. Lett. B **685**, 239 (2010).
[7] C. V. Meister, Astron. Nachr. **312**, 413 (1991).
[8] A. W. Strong, I. V. Moskalenko, and V. S. Ptuskin, Annu. Rev. Nucl. Part. Sci. **57**, 285 (2007).
[9] J. P. Wefel *et al.*, in *Proceedings of the 30th International Cosmic Ray Conference*, (Universidad Nacional Autónoma de México, Mexico, 2008) pp. 31–34.
[10] A. D. Panov *et al.*, Bull. Russ. Acad. Sci.: Phys. **73**, 564 (2009).
[11] H. S. Ahn *et al.*, Astrophys. J. **714**, L89 (2010).
[12] Y. S. Yoon, Astrophys. J. **728**, 122 (2011).
[13] O. Adriani, Science **332**, 69 (2011).
[14] J. Alcaraz *et al.*, Phys. Lett. B **490**, 27 (2000).
[15] S. Haino *et al.*, Phys. Lett. B **594**, 35 (2004).
[16] http://adsabs.harvard.edu/abs/2014arXiv1402.0467C
[17] A. W. Strong, I. V. Moskalenko, and O. Reimer, Astrophys. J. **537**, 763 (2000).
[18] A. W. Strong, I. V. Moskalenko, and O. Reimer, Astrophys. J. **613**, 962 (2004).
[19] T. A. Porter, I. V. Moskalenko, A. W. Strong, E. Orlando, and L. Bouchet, Astrophys. J. **682**, 400 (2008).
[20] A. A. Abdo *et al.*, Phys. Rev. Lett. **103**, 251101 (2009).
[21] M. Ackermann *et al.*, Astrophys. J. **750**, 3 (2012).
[22] A. A. Abdo *et al.*, Astrophys. J. **703**, 1249 (2009).
[23] A. A. Abdo *et al.*, Astrophys. J. **710**, 133 (2010).
[24] D. J. Thompson, G. A. Simpson, and M. E. Ozel, J. Geophys. Res. **86**, 1265 (1981).
[25] D. Petry, in *High Energy Gamma-Ray Astronomy*, edited by F. A. Aharonian, H. J. Völk, and D. Horns, *AIP Conf. Proc. No. 745* (AIP, New York, 2005), pp. 709–714.
[26] A. A. Abdo *et al.*, Phys. Rev. D **80**, 122004 (2009).
[27] The angle between the LAT's boresight and the zenith is called the rocking angle.
[28] J. Bregeon, E. Charles, and M. Wood (Fermi LAT Collaboration), arXiv:1304.5456.
[29] http://fermi.gsfc.nasa.gov/ssc/data/analysis/documentation/Pass7REP_usage.html.
[30] http://fermi.gsfc.nasa.gov/ssc/data/analysis/LAT_caveats.html.
[31] M. Ackermann *et al.*, Astrophys. J. Suppl. Ser. **203**, 4 (2012).
[32] T. Kamae, N. Karlsson, T. Mizuno, T. Abe, and T. Koi, Astrophys. J. **647**, 692 (2006).
[33] C. D. Orth and A. Buffington, Astrophys. J. **206**, 312 (1976).
[34] T. W. Atwater and P. S. Freier, Phys. Rev. Lett. **56**, 1350 (1986).
[35] M. Kachelrieß and S. Ostapchenko, Phys. Rev. D **86**, 043004 (2012).
[36] Work in preparation by the LAT Collaboration.
[37] S. R. Kelner, F. A. Aharonian, and V. V. Bugayov, Phys. Rev. D **74**, 034018 (2006).
[38] J. M. Picone, A. E. Hedin, D. P. Drob, and A. C. Aikin, J. Geophys. Res. **107**, 1468 (2002).